J. Fluid Mech. (2008), *vol.* 594, *pp.* 463–491.
doi:10.1017/S0022112007009202 Printed in the United Kingdom

Vortex-induced vibrations of a circular cylinder at low Reynolds numbers

T. K. PRASANTH AND S. MITTAL†

Department of Aerospace Engineering, Indian Institute of Technology, Kanpur, UP 208 016, India

(Received 21 August 2006 and in revised form 15 September 2007)

Results are presented for a numerical simulation of vortex-induced vibrations of a circular cylinder of low non-dimensional mass ($m^* = 10$) in the laminar flow regime ($60 < Re < 200$). The natural structural frequency of the oscillator, f_N, matches the vortex shedding frequency for a stationary cylinder at $Re = 100$. This corresponds to $f_N D^2/\nu = 16.6$, where D is the diameter of the cylinder and ν the coefficient of viscosity of the fluid. A stabilized space–time finite element formulation is utilized to solve the incompressible flow equations in primitive variables form in two dimensions. Unlike at high Re, where the cylinder response is known to be associated with three branches, at low Re only two branches are identified: 'initial' and 'lower'. For a blockage of 2.5 % and less the onset of synchronization, in the lower Re range, is accompanied by an intermittent switching between two modes with vortex shedding occurring at different frequencies. With higher blockage the jump from the initial to lower branch is hysteretic. Results from free vibrations are compared to the data from experiments for forced vibrations reported earlier. Excellent agreement is observed for the critical amplitude required for the onset of synchronization. The comparison brings out the possibility of hysteresis in forced vibrations. The phase difference between the lift force and transverse displacement shows a jump of almost 180° at, approximately, the middle of the synchronization region. This jump is not hysteretic and it is not associated with any radical change in the vortex shedding pattern. Instead, it is caused by changes in the location and value of the maximum suction on the lower and upper surface of the cylinder. This is observed clearly by comparing the time-averaged flow for a vibrating cylinder for different Re. While the mean flow for Re beyond the phase jump is similar to that for a stationary cylinder, it is associated with a pair of counter-rotating vortices in the near wake for Re prior to the phase jump. The phase jump appears to be one of the mechanisms of the oscillator to self-limit its vibration amplitude.

1. Introduction

Flow past a circular cylinder has been a subject of interest for a long time. Despite its simple geometry, it is associated with rich phenomena, many of which are common to other bluff body flows. It is well known that beyond $Re \sim 47$ the cylinder experiences unsteady aerodynamic forces due to alternate vortex shedding. It can undergo vortex-induced vibrations (VIV) if it is mounted on elastic supports. The cylinder motion can significantly alter the vortex pattern in the wake. A well-known effect is the synchronization/lock-in of the vortex shedding frequency to the oscillation frequency

† Author to whom correspondence shoud be addressed: smittal@iitk.ac.in

of the body over a range of Reynolds numbers. For a comprehensive review of the research on various aspects of vortex-induced vibrations, the reader is referred to the review articles by Williamson & Govardhan (2004), Sarpkaya (1979, 2004) and Bearman (1984).

It is known from the pioneering works of Feng (1968) and Bishop & Hassan (1964) that the lock-in phenomenon is accompanied by jumps in transverse vibration amplitude (A/D) and fluid forces on the body. In addition, the phase difference between the cylinder displacement and fluid forces also shows a sharp change. The exact point of the jump shows hysteresis and depends on whether the point is on the decreasing- or increasing-velocity curve. Khalak & Williamson (1999) conducted experiments involving transverse oscillations of an elastically mounted rigid cylinder at very low mass–damping, $m^*\zeta$ ($5000 \leqslant Re \leqslant 16000$). They showed that, depending on the value of the combined mass–damping parameter the response of the cylinder can be one of two types. For low $m^*\zeta$ the response consists of three branches: initial excitation, upper and lower. The transition between the initial and upper branches involves hysteresis. Intermittent switching of flow modes is observed for the transition between the upper and lower branches. Using flow visualization they have shown that the initial branch is associated with the 2S mode of vortex shedding (classical Kármán street with a single vortex released from each side of the cylinder in one cycle of shedding). The 2P mode of shedding (a vortex pair is released from each side of the cylinder during a cycle of shedding) is observed on the lower branch. Hysteresis with respect to transition between initial and upper branches is observed for a range of reduced velocities ($U^* = 4.45 - 4.70$). The reduced velocity is defined as $U^* = U/fD$, where, U is the free-stream speed, D the diameter of the cylinder, and f the vibrating frequency of the cylinder. For high $m^*\zeta$ only two response branches are seen. This is often referred to as the classical Feng-type response.

Brika & Laneville (1993) in their experimental investigation of VIV of a long flexible circular cylinder with low damping ratio observed hysteresis in the transverse displacement of the cylinder with variation of flow velocity ($3400 \leqslant Re \leqslant 11800$). Two branches of cylinder response were found depending on whether the flow velocity is varied gradually or impulsively. The upper branch is realized when the velocity is increased with small increments. In this case, the 2S mode of vortex shedding is observed. The lower branch is obtained when the velocity is either changed impulsively or decreased gradually. This branch is associated with the 2P mode of vortex shedding as suggested by Williamson & Roshko (1998) from their experiments on forced oscillation of a cylinder.

Williamson & Govardhan (2004) demonstrated, via a compilation of results from the literature for various studies, that hysteresis at the low-velocity end of the synchronization region may exist even in the laminar vortex shedding range. Singh & Mittal (2005) confirmed this via their numerical simulations. They showed for the first time that in the laminar flow regime the hysteresis also exists near the higher U^* end of the lock-in regime. They also showed that the hysteretic behaviour persists even when the cylinder is allowed to oscillate only in the transverse direction. Their computations were carried out for a fixed Reynolds number ($Re = 100$) while the reduced speed was varied. In another computational study, Mittal & Singh (2005) reported that for certain natural frequencies of the spring–mass system, vortex shedding and self-excited vibrations of the cylinder are possible for Re as low as 20.

The cause of hysteresis has been a point of discussion among various researchers. It can be caused either by the nonlinearity of the flow or that of the structural

components such as the springs and damper. Parkinson (1989), by analysing results from Feng (1968), suggested that the hysteresis originates from the fluid system and not from the oscillator. Williamson & Roshko (1988), from their experimental studies, attributed hysteresis to a sudden change in the wake modes such as 2S and 2P. Brika & Laneville (1993) confirmed that the hysteresis is indeed due to the flow and attributed it to the drastic changes in the structure of the vortices that they observed in their experiments. Singh & Mittal (2005), from their computational study, have also observed hysteresis. Since the computational model assumes a linear spring, this confirms that hysteresis can be observed without any nonlinearity in the structural model.

Mittal & Kumar (1999) carried out a computational study at $Re = 325$ for a cylinder that is allowed to vibrate in the in-line and transverse directions. Computations were carried out for various values of the reduced natural frequency, F_N ($= f_N D/U$, where f_N is the natural frequency of the system). Lock-in was observed for a range of the values of F_N. Over a certain range of the structural frequency, the vortex-shedding frequency of the oscillating cylinder did not match F_N exactly; there is a slight detuning. Mittal & Kumar (1999) referred to this phenomenon as *soft-lock-in*. They showed that this detuning disappears when the mass of the cylinder is significantly larger than the mass of the surrounding fluid it displaces. It has also been pointed out by Khalak & Williamson (1999) that, for low m^*, synchronization is characterized by the matching of the vortex-shedding and cylinder vibration frequencies. In general, at synchronization, the vortex-shedding frequency can be quite different from the natural frequency.

The effect of blockage on the flow past a stationary cylinder is relatively well known. For example, Kumar & Mittal (2006*a*, *b*) investigated the effect of blockage on the critical Re at the onset of the primary wake instability. They reported a non-monotonic variation of the critical Re with blockage. It is found that as the blockage increases, the critical Re for the onset of the instability first decreases and then increases. However, a monotonic increase in the non-dimensional shedding frequency at the onset of instability, with increase in blockage, is observed. There have been very few studies to investigate the effect of blockage on flow past an oscillating cylinder. Here, blockage is defined as the ratio of the cylinder diameter to the cross-flow dimension of the wind tunnel/tow tank or the computational domain.

Prasanth *et al.* (2006) in their computations of flow past a vibrating cylinder have shown that even a blockage of 5 % may have a significant effect on the flow. Interestingly, a blockage of this order results in a small effect for the stationary cylinder. Barring the study of Brika & Laneville (1993), which was carried out for a blockage of 1.8 %, the blockage for the investigations discussed above is larger than 5 %. For example, it is 8.3 % for Feng (1968), 8.4 % for Bishop & Hassan (1964). Also, it is 4.2 % and 8.3 % for Carberry, Sheridan & Rockwell (2005) and 10 % for Khalak & Williamson(1996). More details on the blockage used for various experimental studies can be found in Norberg (2003) and Williamson & Govardhan (2004). The blockage for the numerical investigations by Singh & Mittal (2005) is 5 % and is 6.25 % for the study by Mittal & Tezduyar (1992).

In this paper, the effect of blockage on VIV is confirmed by conducting a systematic study at low Re for various values of blockage. Unlike the earlier studies (Singh & Mittal 2005 and Prasanth *et al.* 2006) the computations here are conducted for a system that is closer to a physical experiment; f_N is fixed. For the first time, it is shown that the hysteresis at the lower Re range of lock-in reduces with a decrease in blockage and disappears for blockages of 2.5 % and less.

Another interesting feature observed in various forced vibration studies is the sudden jump in phase between the transverse displacement and lift force. This was first reported by Bishop & Hassan (1963). Ongoren & Rockwell (1988*a*, *b*), in their forced vibration experiments, have observed a phase shift of $\sim 180^\circ$ when the frequency ratio f_e/f_0 was increased through unity. Here f_e is the excitation frequency and f_0 is the natural shedding frequency. During this transition, a switch in the phase of the initially shed vortex to the opposite side of the cylinder is observed. Carberry, Sheridan & Rockwell (2001) observed an abrupt phase shift of the order of 180° with increase in the frequency of oscillation. In their study, the cylinder was forced to oscillate close to the Kármán frequency. The jump in phase was also associated with a sudden jump in the lift force and a change in the mode of vortex shedding. Gu, Chyu & Rockwell (1994) studied the timing of vortex formation in forced oscillations of a cylinder. They observed a dramatic change in phase because of the abrupt switching of the vorticity concentration to the opposite side of the cylinder. This was confirmed by Lu & Dalton (1996) from numerical calculations. Blackburn & Henderson (1999), from their two-dimensional numerical study at $Re = 500$, proposed that the discontinuous switch in phase of vortex shedding is the outcome of a competition between two vorticity production mechanisms. They also demonstrated that the switch is associated with a change in sign of mechanical energy transfer between the cylinder and the flow. In all the above cases of forced vibration studies, the phase angle is found to be either 0° or 180°, approximately.

Free vibrations can be significantly different from forced vibrations. In the case of vortex-induced oscillation the motion of the cylinder is intrinsically coupled with the wake structure, which makes it more complex than forced vibration. In forced vibrations, one is looking at the wake structure caused by the predefined movement of the cylinder. Al Jamal & Dalton (2005), via two-dimensional large-eddy simulations, reported that in the case of self-excited oscillation in the intermediate Re range ($Re = 8000$) the phase angle can possibly vary a great deal because of more irregular oscillation. Khalak & Williamson (1999), in their study of vortex-induced vibrations at low mass–damping observed that the 180° jump in phase angle takes place only when the flow jumps between upper–lower branches of response. Govardhan & Williamson (2000) defined two phase angles: vortex phase ϕ_{vortex} between vortex force and displacement and total phase ϕ_{total} between total force and displacement. They demonstrated that the first mode transition (initial to upper) involves a jump in ϕ_{vortex}, which is associated with a jump from a 2S to a 2P vortex wake mode and a corresponding switch in vortex shedding timing. Across the second mode transition (upper–lower), there is a jump in ϕ_{total}. Here, there is no jump in ϕ_{vortex} as it is not associated with any switch in timing of vortex shedding. Both upper and lower branches are associated with the 2P mode of shedding. They also concluded that in the case of high mass–damping, the switch in the timing coincides with the jump in total phase (ϕ_{total}). In his review article, Sarpkaya (2004) pointed out that in a viscous medium, the added-mass coefficient is very important in determining the phase jump when the non-dimensionalized mass, m^*, is small. It was shown that a 180° phase shift corresponds to a change in sign of the added mass from positive to negative or vice versa, depending on the direction of change of f_{ex} (the dimensional frequency of oscillation of cylinder during lock-in).

There are some differences between free vibrations in the laminar regime and at relatively higher Re. The maximum amplitude of transverse oscillations at low Re in the laminar regime is $\sim 0.6D$. This is significantly smaller than that observed at larger Reynolds numbers. Leontini, Thompson & Hourigan (2005) in a recent numerical

study of flow past an elastically mounted cylinder at $Re = 200$ have reported a comparison between the high- and low-Reynolds-number effects. They suggested that the genesis of higher-Re three-dimensional behaviour such as an upper branch can be seen in lower-Re two-dimensional flows. Their frequency response shows a pseudo-upper branch when compared to the results of Khalak & Williamson (1999). The phase difference between lift force and displacement, ϕ, shows an initial jump of 45° and then an almost linear climb to around 120°. But a lower m^* was found to show a similar behaviour of ϕ as observed in Khalak & Williamson(1999), i.e. a sudden jump in ϕ from almost 0° to 180° was observed. In this work we investigate the phase between lift and cylinder response at low Reynolds numbers for free vibrations. In particular we seek answers to the following questions. Does a jump in ϕ occur at low Re? Is it accompanied by a change in the mode of vortex shedding? What are the implications of the jump in ϕ?

The outline of the rest of the article is as follows. We begin by reviewing the governing equations for incompressible fluid flow and a rigid oscillator on spring supports in § 2. Section 3 describes the stabilized space–time finite element formulation (Tezduyar *et al.* 1992*a*, *b*) utilized to solve the governing equations. The SUPG (streamline-upwind/Petrov–Galerkin) and PSPG (pressure-stabilizing/Petrov–Galerkin) stabilization technique (Tezduyar *et al.* 1992*c*) is employed to stabilize our computations against spurious numerical oscillations and to enable us to use equal-order-interpolation velocity–pressure elements. The problem set-up is defined along with the boundary and initial conditions in § 4. In this section we also describe the mesh moving scheme that we use to accommodate the motion of the cylinder. In § 5 we demonstrate the validity of the formulation in computing such flows and establish the adequacy of the finite element mesh and location of computational boundaries in computing free vibrations. In addition to studying the variation of peak amplitude with Re we include the variation of r.m.s. values of cylinder response. The effect of blockage on the hysteretic *vs.* intermittent behaviour is very clearly seen on the plots with r.m.s. values. This suggests that the plots with r.m.s. values may be more meaningful in VIV than the ones with maximum amplitude. The large unsteady variation of aerodynamic coefficients is explained via time variation of the pressure distribution on the cylinder surface.

In § 6 the response of the cylinder and variation of aerodynamic coefficients along with the synchronization and various branches associated with vortex-induced vibration at low Re are presented. Section 7 includes a comparison of free vibration results with forced vibration data from Koopmann (1967). For the first time, the comparison of the free and forced vibration data is presented on a Y_{max}/D *vs.* f^* plot to bring out the differences between the two. The various modes of vortex shedding and their variation with cylinder vibrations is discussed in § 8. During the transition from the 'initial' to 'lower' branch, for low blockage, switching between two modes of vortex shedding takes place. The difference in the frequency of vortex shedding of the two modes is captured and confirmed via a Hilbert transform for the first time for low-Re flows. Next, in § 9 we look at the variation of phase between lift force and cylinder displacement with Re. We show, for low Re, that the phase jump occurs at the point where f^* reaches a value exactly equal to 1 (and not during the transition between the initial and lower branch). Unlike at large Re, the phase jump is not related to a change in the mode of vortex shedding. Instead, it is found to be related to the pressure variations. Decomposition of the flow into time-averaged and time-varying components reveals that the intense movement of the stagnation and peak suction points for the Re associated with large-amplitude vibrations modifies

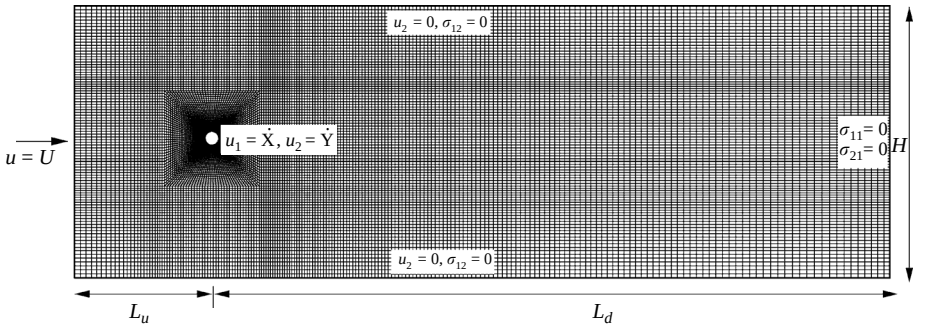

FIGURE 1. A typical finite element mesh for the 5 % blockage with 23 644 nodes and 23 280 quadrilateral elements. The location of the various boundaries and the boundary conditions are also shown.

the time-averaged flow significantly. It is found that even though the instantaneous flows for Re on either side of the phase jumps are very similar, the time-averaged and unsteady components exhibit substantial differences. Further, it is shown that the phase jump is a mechanism to self-limit the amplitude of cylinder response in free vibrations. We end with a few concluding remarks in § 10.

2. The governing equations

2.1. *The incompressible flow equations*

Let $\Omega_t \subset \mathbb{R}^{n_{sd}}$ and $(0, T)$ be the spatial and temporal domains respectively, where n_{sd} is the number of space dimensions, and let Γ_t denote the boundary of Ω_t. The spatial and temporal coordinates are denoted by $\boldsymbol{x}$ and t. The Navier–Stokes equations governing incompressible fluid flow are

$$\rho\left(\frac{\partial \boldsymbol{u}}{\partial t} + \boldsymbol{u}\cdot\boldsymbol{\nabla}\boldsymbol{u} - \boldsymbol{f}\right) - \boldsymbol{\nabla}\cdot\boldsymbol{\sigma} = 0 \quad \text{on } \Omega_t \times (0, T), \tag{2.1}$$

$$\boldsymbol{\nabla}\cdot\boldsymbol{u} = 0 \quad \text{on } \Omega_t \times (0, T). \tag{2.2}$$

Here ρ, $\boldsymbol{u}$, $\boldsymbol{f}$ and $\boldsymbol{\sigma}$ are the density, velocity, body force and the stress tensor, respectively. The stress tensor is written as the sum of its isotropic and deviatoric parts:

$$\boldsymbol{\sigma} = -p\boldsymbol{I} + \boldsymbol{T}, \quad \boldsymbol{T} = 2\mu\boldsymbol{\varepsilon}(\boldsymbol{u}), \quad \boldsymbol{\varepsilon}(\boldsymbol{u}) = \tfrac{1}{2}((\boldsymbol{\nabla}\boldsymbol{u}) + (\boldsymbol{\nabla}\boldsymbol{u})^T), \tag{2.3}$$

where p and μ are the pressure and dynamic viscosity, respectively. Both the Dirichlet and Neumann-type boundary conditions are accounted for, represented as

$$\boldsymbol{u} = \boldsymbol{g} \text{ on } (\Gamma_t)_g, \quad \boldsymbol{n}\cdot\boldsymbol{\sigma} = \boldsymbol{h} \text{ on } (\Gamma_t)_h, \tag{2.4}$$

where $(\Gamma_t)_g$ and $(\Gamma_t)_h$ are complementary subsets of the boundary Γ_t and $\boldsymbol{n}$ is its unit normal vector. The details of the boundary conditions for the present problem are shown in figure 1 and given in § 4. For the freely vibrating cylinder the velocity of the fluid on the cylinder surface is determined by solving the equations of motion for a spring-mounted oscillator. The initial condition on the velocity is specified on Ω_t at $t = 0$:

$$\boldsymbol{u}(\boldsymbol{x}, 0) = \boldsymbol{u}_0 \quad \text{on } \Omega_0, \tag{2.5}$$

where $\boldsymbol{u}_0$ is divergence free.

2.2. *The equations of motion for a rigid body*

A solid body immersed in fluid experiences unsteady forces and in certain cases may exhibit rigid body motion. The motion of the body, in the two directions along the Cartesian axes, is governed by the following equations:

$$\ddot{X} + 4\pi F_N \zeta \dot{X} + (2\pi F_N)^2 X = \frac{2C_D}{\pi m^*} \qquad \text{for } (0, T), \tag{2.6}$$

$$\ddot{Y} + 4\pi F_N \zeta \dot{Y} + (2\pi F_N)^2 Y = \frac{2C_L}{\pi m^*} \qquad \text{for } (0, T). \tag{2.7}$$

Here, F_N is the reduced natural frequency of the oscillator, ζ the structural damping ratio, m^* the non-dimensional mass of the body while C_L and C_D are the instantaneous lift and drag coefficients for the body, respectively. The free-stream flow is assumed to be along the x-axis. $\ddot{X}$, $\dot{X}$ and X denote the normalized in-line acceleration, velocity and displacement of the body, respectively, while $\ddot{Y}$, $\dot{Y}$ and Y represent the same quantities associated with the cross-flow motion. In the present study, in which the rigid body is a circular cylinder, the displacement and velocity are normalized by the diameter, D, of the cylinder and the free-stream speed, U, respectively. The reduced natural frequency of the system, F_N is defined as $f_N D/U$ where f_N is the natural frequency of the oscillator. Another related parameter is the reduced velocity, U^*. It is defined as $U^* = U/(f_N D) = 1/F_N$.

The non-dimensional mass of the cylinder is defined as $m^* = 4m/(\pi\rho D^2)$ where m is the actual mass of the oscillator per unit length and ρ is the density of the fluid. The force coefficients are computed by carrying an integration, that involves the pressure and viscous stresses, around the circumference of the cylinder.

3. The finite element formulation

To accommodate the motion of the cylinder and the deformation of the mesh, a formulation that can handle moving boundaries and interfaces is employed. In order to construct the finite element function spaces for the space–time method, we partition the time interval $(0, T)$ into subintervals $I_n = (t_n, t_{n+1})$, where t_n and t_{n+1} belong to an ordered series of time levels: $0 = t_0 < t_1 < \cdots < t_N = T$. Let $\Omega_n = \Omega_{t_n}$ and $\Gamma_n = \Gamma_{t_n}$. We define the space–time slab Q_n as the domain enclosed by the surfaces Ω_n, Ω_{n+1}, and P_n, where P_n is the surface described by the boundary Γ_t as t traverses I_n. As is the case with Γ_t, the surface P_n is decomposed into $(P_n)_g$ and $(P_n)_h$ with respect to the type of boundary condition (Dirichlet or Neumann) being imposed. For each space–time slab we define the corresponding finite element function spaces: $(\mathscr{S}^h_{\mathbf{u}})_n$, $(\mathscr{V}^h_{\mathbf{u}})_n$, $(\mathscr{S}^h_p)_n$, and $(\mathscr{V}^h_p)_n$. Over the element domain, this space is formed by using first-order polynomials in space and time. Globally, the interpolation functions are continuous in space but discontinuous in time.

The stabilized space–time formulation for deforming domains is then written as follows: given $(\boldsymbol{u}^h)_{n^-}$, find $\boldsymbol{u}^h \in (\mathscr{S}^h_{\mathbf{u}})_n$ and $p^h \in (\mathscr{S}^h_p)_n$ such that $\forall \boldsymbol{w}^h \in (\mathscr{V}^h_{\mathbf{u}})_n$, $q^h \in (\mathscr{V}^h_p)_n$:

$$\int_{Q_n} \boldsymbol{w}^h \cdot \rho \left(\frac{\partial \boldsymbol{u}^h}{\partial t} + \boldsymbol{u}^h \cdot \boldsymbol{\nabla} \boldsymbol{u}^h - \boldsymbol{f} \right) \mathrm{d}\Omega + \int_{Q_n} \boldsymbol{\varepsilon}(\boldsymbol{w}^h) : \boldsymbol{\sigma}(p^h, \boldsymbol{u}^h) \, \mathrm{d}Q + \int_{Q_n} q^h \boldsymbol{\nabla} \cdot \boldsymbol{u}^h \, \mathrm{d}Q$$
$$+ \sum_{e=1}^{n_{el}} \int_{Q_n^e} \frac{1}{\rho} \tau \left[\rho \left(\frac{\partial \boldsymbol{w}^h}{\partial t} + \boldsymbol{u}^h \cdot \boldsymbol{\nabla} \boldsymbol{w}^h \right) - \boldsymbol{\nabla} \cdot \boldsymbol{\sigma}(q^h, \boldsymbol{w}^h) \right]$$

$$\cdot \left[\rho\left(\frac{\partial \boldsymbol{u}^h}{\partial t} + \boldsymbol{u}^h \cdot \boldsymbol{\nabla}\boldsymbol{u}^h - \boldsymbol{f}\right) - \boldsymbol{\nabla}\cdot\boldsymbol{\sigma}(p^h, \boldsymbol{u}^h)\right] \mathrm{d}Q$$
$$+ \sum_{e=1}^{n_{el}} \int_{Q_n^e} \delta \boldsymbol{\nabla}\cdot\boldsymbol{w}^h \rho \boldsymbol{\nabla}\cdot\boldsymbol{u}^h \mathrm{d}Q + \int_{\Omega_n} (\boldsymbol{w}^h)_n^+ \cdot \rho\left((\boldsymbol{u}^h)_n^+ - (\boldsymbol{u}^h)_n^-\right) \mathrm{d}\Omega = \int_{(P_n)_h} \boldsymbol{w}^h \cdot \boldsymbol{h}^h \mathrm{d}P. \tag{3.1}$$

This process is applied sequentially to all the space–time slabs $Q_0, Q_1, \ldots, Q_{N-1}$. In the variational formulation given by (3.1), the following notation is being used:

$$(\boldsymbol{u}^h)_n^{\pm} = \lim_{\varepsilon \to 0} \boldsymbol{u}(t_n \pm \varepsilon), \tag{3.2}$$

$$\int_{Q_n} (\ldots)\,\mathrm{d}Q = \int_{I_n}\int_{\Omega_n} (\ldots)\,\mathrm{d}\Omega\,\mathrm{d}t, \tag{3.3}$$

$$\int_{P_n} (\ldots)\,\mathrm{d}P = \int_{I_n}\int_{\Gamma_n} (\ldots)\,\mathrm{d}\Gamma\,\mathrm{d}t. \tag{3.4}$$

The computations start with

$$(\boldsymbol{u}^h)_0^- = \boldsymbol{u}_0, \tag{3.5}$$

where $\boldsymbol{u}_0$ is divergence free.

The variational formulation given by (3.1), includes certain stabilization terms added to the basic Galerkin formulation to enhance its numerical stability. Details on the formulation, including the definitions of the coefficients τ and δ, can be found in the papers by Tezduyar *et al.* (1992*a*, *b*, *c*). The equations of motion for the oscillator given by (2.6)–(2.7) are also cast in the space–time formulation in the manner described in Tezduyar *et al.* (1992*c*) and Mittal (1992).

4. Problem description

The cylinder is mounted on elastic supports and is free to undergo transverse as well as streamwise vibrations. Re is based on the free-stream speed (U), diameter of the cylinder (D) and viscosity of the fluid. The non-dimensional mass of the cylinder is $m^* = 10.0$. To encourage high-amplitude oscillations, the structural damping coefficient is set to zero. The springs in both the transverse and in-line directions are assumed to be identical and exhibit linear behaviour. Singh & Mittal (2005) carried out computations for free vibrations for two sets of parameters: (*a*) Re is fixed (=100) and F_N is varied; (*b*) F_N is fixed (= 1/4.92) and Re is varied. The computations were carried out for only one value of blockage ($B = 5\,\%$). Prasanth *et al.* (2006) presented results for $Re = 100$ and varying F_N for 1 % and 5 % blockage. In the present work, it is assumed that the dimensional natural frequency, f_N, of the spring–mass system does not vary with flow speed. As as result, F_N varies with Re. Compared to the situations in Singh & Mittal (2005) and Prasanth *et al.* (2006) the present situation is much closer to an experimental set-up. The mass of the oscillator and the spring stiffness are chosen such that the natural structural frequency matches the vortex shedding frequency of a stationary cylinder at $Re = 100$. This corresponds to the variation in the non-dimensional natural frequency of the oscillator with Re as $F_N = 16.6/Re$. With these choice of parameters the flow stays in the regime in which it is expected to be two-dimensional and laminar.

4.1. *Boundary conditions*

The no-slip condition is applied to the velocity at the cylinder surface. The location of the cylinder and the flow velocity on its surface are updated at each nonlinear iteration of the solution to the flow equations. Free-stream values are assigned for the velocity at the upstream boundary and the stress vector is set to zero at the downstream boundary. This type of an outflow boundary condition is often known as the 'traction free' condition. On the upper and lower boundaries, the component of the velocity normal to, and the component of the stress vector along, the boundaries are prescribed a zero value. The boundary conditions are also shown in figure 1.

4.2. *Finite element mesh and mesh moving scheme*

The cylinder is placed in a rectangular computational domain whose upstream and downstream boundaries are located at distance L_u and L_d from the centre of the cylinder. The lateral boundaries are separated by a distance H. The blockage ratio, B, is defined as $B = D/H$. Figure 1 shows a typical finite element mesh for 5 % blockage. The mesh moving scheme has been designed such that the mesh in the square box around the cylinder moves along with it as a rigid body. The location of the outer boundary is fixed. As a result, the movement of the cylinder causes deformation of the mesh points lying between the square region and the outer boundary. This kind of mesh movement is expected to lead to almost no projection errors in the flow close to the cylinder. This scheme has been used in our earlier work; for example, in Mittal & Kumar (1999) for single cylinder and in Mittal & Kumar (2001) for a pair of cylinders.

5. Validation of method and convergence of results

Equal-in-order basis functions for velocity and pressure, that are bilinear in space and linear in time, are used and $2 \times 2 \times 2$ Gaussian quadrature is employed for numerical integration. The nonlinear equation systems resulting from the finite-element discretization of the flow equations are solved using the Generalized Minimum RESidual (GMRES) technique in conjunction with diagonal preconditioners. In all the figures for the vorticity field presented in this article, a grey scale based on the magnitude of vorticity is used for shading. The darker shades of grey represents higher values of vorticity. To differentiate between positive and negative values, iso-vorticity contours are also shown. Black contour lines represent negative values of the vorticity field, while the white lines show positive values.

$Re = 100$ flow past a stationary cylinder was reported by Singh & Mittal (2005) for various values of blockage. Excellent agreement with aerodynamic coefficients reported by other researchers is observed. It was also found that a blockage of 5 % does not have any significant effect on the $Re = 100$ flow past a stationary cylinder. Next, the case of free vibrations is considered. The $Re = 100$ ($U^* \sim 6.0$) flow lies on the maximum amplitude branch of the cylinder oscillations. It is associated with a large wake width. This case is utilized to investigate the effect of mesh resolution and streamwise location of computational boundaries.

5.1. *Effect of mesh resolution*

Two finite element meshes are utilized to solve the $Re = 100$ flow past a freely vibrating cylinder. The details of the finite element mesh and a summary of the response of the cylinder and the aerodynamic coefficients are given in table 1. For both the cases, the time step, Δt is 0.0625 and the domain size is identical ($L_u/D = 10$, $L_d/D = 25.5$ and

Mesh	Nodes	Elements	St	Y_{max}/D	X_{rms}/D	$\bar{X}/D$	$C_{L_{max}}$	$C_{D_{rms}}$	$\bar{C}_D$
M7k	7437	7236	0.1643	0.516	0.00494	0.1115	0.1929	0.2486	1.90
M15k	15004	14710	0.1644	0.503	0.00484	0.1100	0.1900	0.2434	1.88

TABLE 1. $Re = 100$ flow past a freely vibrating cylinder: effect of mesh resolution. The other parameters for the computations are $\Delta t = 0.0625$, $L_u/D = 10$, $L_d/D = 25.5$ and $B = 5\,\%$.

Mesh	Nodes	L_u/D	St	Y_{max}/D	X_{rms}/D	$\bar{X}/D$	$C_{L_{max}}$	$C_{D_{rms}}$	$\bar{C}_D$
M7k	7437	10.0	0.1643	0.516	0.00494	0.1115	0.1929	0.2486	1.90
M7k2	7779	15.0	0.1642	0.516	0.00500	0.1110	0.2087	0.2507	1.90
M9k	9603	25.0	0.1644	0.516	0.00505	0.1110	0.2090	0.2550	1.90

TABLE 2. $Re = 100$ flow past a freely vibrating cylinder: effect of the location of upstream boundary L_u/D. The other parameters for the computations are $L_d/D = 25.5$ and $B = 5\,\%$.

$B = 5\,\%$). The initial condition for the simulations is the fully developed unsteady flow past a stationary cylinder at the same Re. It is observed that the two meshes result in very similar solutions. From table 1 it is seen that the largest deviation between the two sets of results is for the maximum amplitude in transverse oscillation ($\sim 2.5\,\%$). This establishes the adequacy of mesh $M7k$ in computing the flow past a freely vibrating cylinder.

5.2. *Effect of time step size*

Computations are carried out for two different values of time step to study its influence on flow past a freely vibrating cylinder. The difference in the maximum transverse oscillation of the cylinder obtained with $\Delta t = 0.0625$ and 0.0125 is 0.4 %, approximately. Therefore, a time step of $\Delta t = 0.0625$ is used for all the calculations in this paper.

5.3. *Effect of the streamwise location of the computational boundaries*

The effect of the location of both the upstream and downstream boundary on free vibrations of the cylinder at $Re = 100$ is investigated.

Location of upstream boundary

Computations are carried for three locations of the upstream boundary, L_u/D. The details of the finite element meshes and the results obtained with them are listed in table 2. For all the meshes the location of the downstream boundary and blockage are identical ($L_d/D = 25.5$, $B = 5\,\%$). The results from the three sets of computations are very similar. Although the maximum lift coefficient is slightly underpredicted for $L_u/D = 10$, the amplitude of cylinder response predicted by all three meshes is in excellent agreement.

Location of downstream boundary

The details of the finite element mesh employed to study the effect of L_d/D and a summary of the response of the cylinder and aerodynamic coefficients are given in table 3. Both meshes are associated with the same blockage and location of upstream boundary ($B = 5\,\%$, $L_u/D = 10$). It is clear from Table 3 that the results from both the meshes are virtually identical. This reflects the adequacy of $L_d/D = 25.5$ in computing the near wake flow and free vibrations of a cylinder for $Re = 100$.

Mesh	Nodes	L_d/D	St	Y_{max}/D	X_{rms}/D	$\bar{X}/D$	$C_{L_{max}}$	$C_{D_{rms}}$	$\bar{C}_D$
M7k	7437	25.5	0.1643	0.516	0.00494	0.1115	0.1929	0.2486	1.90
M23k	23644	50.0	0.1642	0.510	0.00494	0.1105	0.1950	0.2484	1.89

TABLE 3. $Re = 100$ flow past a freely vibrating cylinder: effect of location of downstream boundary L_d/D. The other parameters for the computations are $L_u/D = 10$ and $B = 5\,\%$.

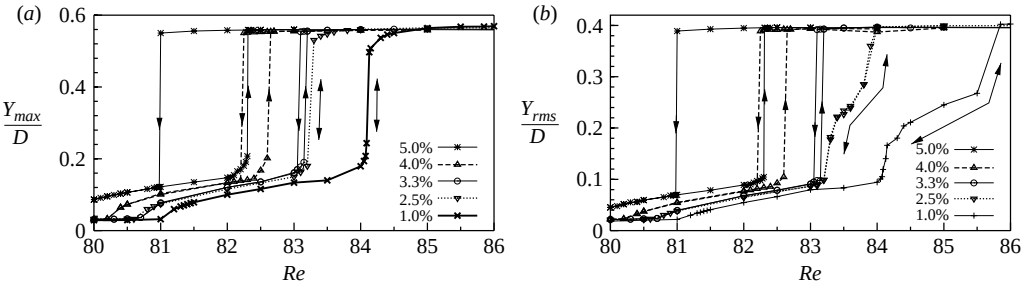

FIGURE 2. Variation of (*a*) the maximum and (*b*) r.m.s. value of transverse displacement of the cylinder with Re for various blockage values close to the lower-Re end of lock-in.

5.4. *Effect of transverse location of the computational boundaries*

The effect of blockage on vortex-induced vibration has not received much attention. Prasanth *et al.* (2006) found that the blockage has a very significant effect on the response of a cylinder undergoing free vibrations. We are aware of only one other study where the effect of blockage for vibrating cylinders has been reported: the dependence of the hysteresis on blockage was observed by Stansby (1976) in his experimental study on forced vibrations of cylinders. Two models were used, with blockage, based on the tunnel width and diameter of the cylinder, of 3.6 % and 7.2 %. Hysteresis was observed only with the model with larger blockage.

To investigate the effect of blockage on free vibrations computations with various values ($B = 5\,\%$, $4\,\%$, $3.33\,\%$ $2.5\,\%$ and $1\,\%$) are carried out. The variation of the normalized maximum amplitude of the transverse oscillations for different blockages, near the lower Re range of the synchronization, is shown in figure 2(*a*). It is seen that the width of the hysteresis loop reduces with a decrease in blockage. For blockage of 2.5 % and less the hysteretic behaviour completely disappears. A similar behaviour is observed for in-line oscillations and aerodynamic coefficients. In general, the jump in cylinder response and aerodynamic coefficients occurs at a slightly smaller Re with increase in blockage. This can be attributed to the increased local acceleration of the flow as blockage increases. Figure 2(*b*) shows the variation of the r.m.s. value of the transverse oscillations of the cylinder with Re near the lower Re end of lock-in. The behaviour at low blockage is found to be qualitatively different from that at high blockage. For example, for the low blockage the increase in the r.m.s. value of the response amplitude takes place in three stages: a steep jump followed by a relatively gradual change and then a sharp jump again. The second stage with more gradual change becomes smaller with increase in blockage and eventually disappears for $B = 3.3\,\%$ and higher. Most of the results in the remainder of the paper are computed with 1 % blockage.

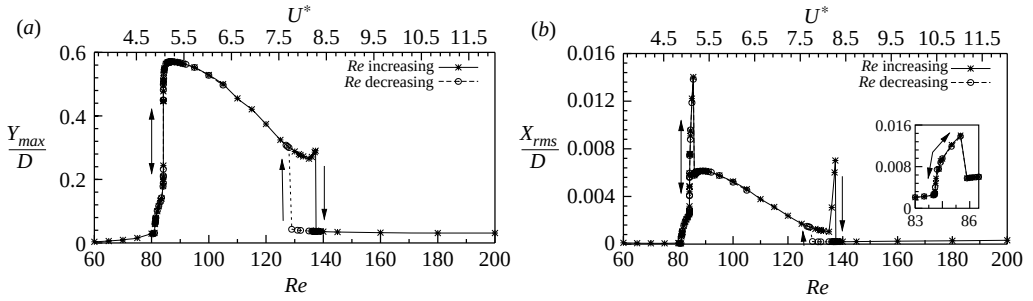

FIGURE 3. Variation of (*a*) maximum transverse oscillation amplitude and (*b*) r.m.s. value of the in-line oscillation amplitude of the cylinder with Re for 1 % blockage.

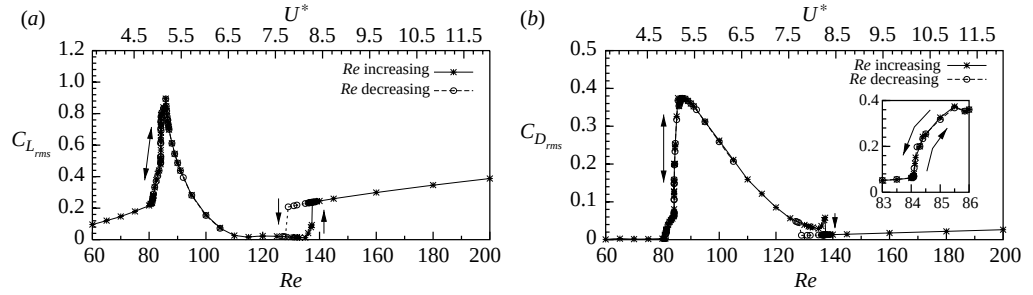

FIGURE 4. Variation of the r.m.s. value of the lift and drag coefficients with Re for 1 % blockage.

6. Free vibrations

6.1. *Cylinder response*

Figure 3 shows the the variation of the transverse as well as the in-line response of the cylinder with Re (and U^*). From figure 3(*a*) it is observed that the peak amplitude of transverse vibration is $0.6D$, approximately. This is in good agreement with the value reported by other researchers for this low-Re regime. Figure 3(*b*) shows the variation of the r.m.s. value of the in-line oscillation normalized with the diameter of the cylinder. As expected, the amplitude of the transverse vibration is significantly higher than that of in-line oscillations. Both the lower and higher Re ends of synchronization are associated with large amplitudes. The r.m.s. value shows a gradual variation near the lower Re end of synchronization. Hysteretic behaviour is observed only at the higher Re end of synchronization.

6.2. *Aerodynamic coefficients*

The variation of the aerodynamic coefficients is shown in figure 4. The very significant effect of vibrations on the aerodynamic forces is quite apparent from this figure. Hysteresis in the force coefficients shows the same trend as the one observed for cylinder response. Compared to a stationary cylinder, the vibrating cylinder experiences much larger lift force close to the lower Re range of synchronization. However, the trend is the opposite at the higher Re range of synchronization. Beyond $Re \sim 90$ the lift coefficient experienced by the vibrating cylinder is smaller than that felt by a stationary one. The r.m.s. value of lift coefficient for a stationary cylinder is found to be approximately 1.25 times that for the freely vibrating case beyond the synchronization region ($Re > 140$). The maximum r.m.s. value of drag coefficient

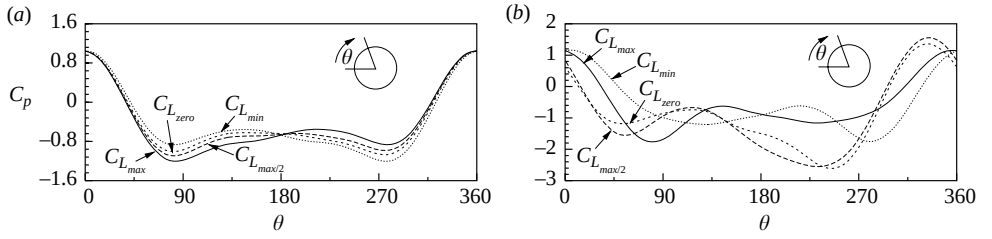

FIGURE 5. $Re = 90$ flow past (a) a stationary and (b) a freely vibrating cylinder: variation of the pressure distribution on the cylinder surface at various time instants during one cycle of lift coefficient.

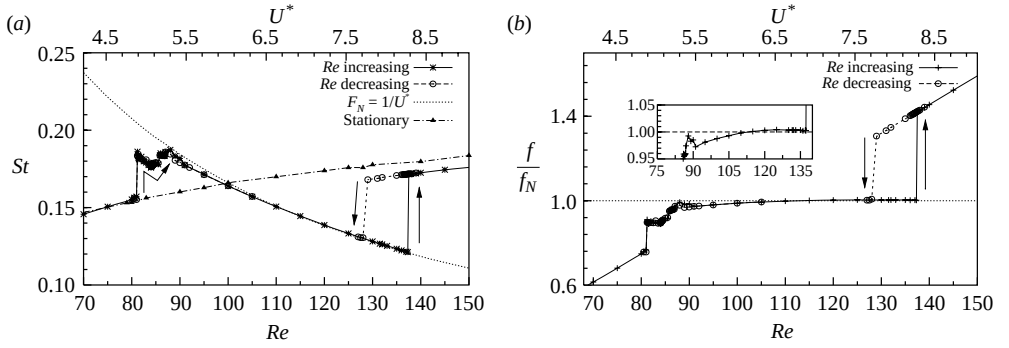

FIGURE 6. Variation of (a) the non-dimensional vortex shedding frequency and (b) the frequency ratio, f/f_N, with Re for 1 % blockage. Also shown is the reduced natural frequency, $F_N = 1/U^*$, and St for the stationary cylinder.

is found to be 0.4 which is very large compared to that for a stationary cylinder. To investigate this, we study the variation of the pressure on the cylinder surface. Figure 5 shows the distribution of the pressure coefficient, C_p, on the cylinder surface for the stationary and moving cylinders at four time instants during a cycle of time variation of C_L for the $Re = 90$ flow. It is found that while the front stagnation point for the stationary cylinder moves very little, it has a substantial movement along the cylinder surface for a vibrating cylinder. Also, the vibrating cylinder is associated with very large changes in the base pressure coefficient during the lift cycle. This leads to a very large time variation of C_D and hence large value of $C_{D_{rms}}$ for the vibrating cylinder.

6.3. *Synchronization and branches of cylinder response*

Figure 6(a) shows the variation of the non-dimensional vortex shedding frequency with Re. The non-dimensional natural frequency, F_N, along with the non-dimensional vortex shedding frequency for a stationary cylinder is also shown in the same figure. The vortex shedding frequency for the vibrating cylinder is affected by its motion for a wide range of Re.

A useful quantity to study in free vibrations is the frequency ratio, f/f_N, shown in figure 6(b). Here, f is the vortex shedding frequency of the vibrating cylinder. It has been pointed out in the literature (Khalak & Williamson 1999 and Williamson & Govardhan 2004) that synchronization/lock-in is defined as the state when the frequency of the periodic wake vortex mode matches the cylinder oscillation frequency. These two frequencies may, however, be different from the natural frequency of the

spring–mass system, i.e. f/f_N need not be necessarily equal to 1.0 at lock-in. The departure of the vortex shedding frequency for the vibrating cylinder from the shedding frequency for a stationary cylinder for a broad range of Re during lock-in is quite apparent from figure 6. It is also seen that outside the lock-in region, the vortex shedding frequency of stationary cylinder shows a small offset from the vortex shedding frequency of the freely oscillating cylinder. This is mainly caused by the oscillation of the cylinder and associated change in vortex shedding timing, especially at the higher Reynolds numbers ($Re > 140$).

At the lower Re end of the synchronization region, the jump in f/f_N occurs in two stages. The first jump occurs at $Re \sim 81$ and signifies the beginning of the synchronization. Using the terminology of Khalak & Williamson (1996), this corresponds to the onset of the 'initial branch'. The vortex shedding frequency for the vibrating cylinder is much larger than that for a stationary cylinder but is smaller than the natural frequency. In the second stage, the vortex shedding frequency gradually approaches the natural frequency. The proximity of f/f_N to unity leads to an increase in the amplitude of cylinder oscillations. At $Re \sim 88$ the cylinder attains the maximum amplitude of oscillation and this marks the onset of the 'lower' branch. Details on the flow characteristics in these regimes are presented later in the paper. At the higher Re end of the synchronization region, the vortex shedding frequency jumps back to that observed for a stationary cylinder. It is found that this jump is hysteretic irrespective of the blockage.

Khalak & Williamson (1996), in their laboratory experiments conducted at much higher Reynolds numbers for a low mass-damping oscillator, reported three branches of cylinder response. The first transition from the 'initial' to the 'upper' branch is associated with a jump in f/f_N and cylinder response and is hysteretic in nature. The second transition is from the 'upper' to 'lower' branch and involves intermittent switching. A final jump in f/f_N marks the end of the synchronization regime. In contrast, at low Re, the upper branch of the cylinder response does not exist.

An interesting observation from figure 6 is regarding the value of Re for which f/f_N assumes a value exactly equal to one. Recall that the mass and the stiffness of the oscillator has been designed to match the vortex shedding frequency for a stationary cylinder at $Re = 100$. Although f/f_N is nearly equal to one for a large range of Re, it assumes the exact value of 1.0 at $Re \sim 110$ which is approximately midway in the range of Re for which lock-in is observed. It is shown later in the paper that the phase between the lift force on the cylinder and its response experiences a $\sim 180^\circ$ jump at the same Reynolds number.

7. Free versus forced vibrations: lock-in boundaries

7.1. *Forced vibrations: data from Koopmann* (1967)

Several researchers in the past have attempted to understand free vibrations via controlled experiments with forced sinusoidal oscillations of a cylinder in a free-stream flow. A review of some of the issues and the corresponding references may be found in Williamson & Govardhan (2004). Koopmann (1967) carried out laboratory experiments to determine the minimum oscillation amplitude required to achieve lock-in for various frequencies of forced vibrations of a cylinder and various Reynolds numbers. Some of the results from his work are shown in figure 7. The x-axis shows f^*, defined as the ratio of the cylinder oscillation frequency (f) and the vortex shedding frequency for a stationary cylinder (f_0). For each f^* there exists a critical oscillation amplitude beyond which the vortex shedding frequency locks into the oscillation

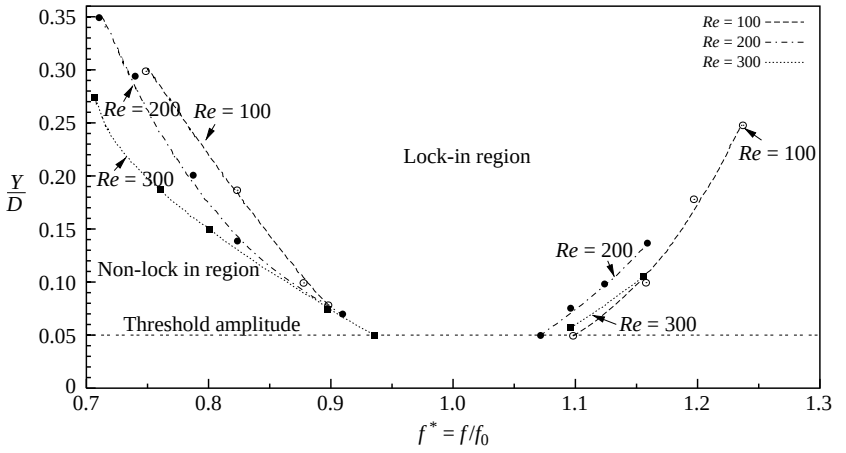

FIGURE 7. Experimental data (from Koopmann 1967) for forced vibrations of a cylinder: critical amplitude of vibrations needed for lock-in for various values of frequency ratio, $f^* = f/f_0$. f and f_0 are the vortex shedding frequency for the vibrating and stationary cylinder, respectively.

frequency. This critical oscillation amplitude is shown on the y-axis. As expected, the oscillation amplitude required for lock-in increases with the increase in the departure of f/f_0 from 1.0. The effect of Re in the laminar flow regime is also shown in the figure. Although there is some effect of Re the general behaviour is quite similar. The threshold amplitude shown in figure 7 is the smallest vibration amplitude of the cylinder for which lock-in is observed. From the flow pictures given in Koopmann (1967) it appears that the presence of the threshold amplitude is associated with the influence of end effects and transition from slantwise to parallel shedding.

7.2. *Free versus forced vibrations*

A question that comes to mind is whether there is any consistency between the amplitude of cylinder oscillations at the onset of lock-in for free and forced vibrations. A plot of the variation of cylinder oscillation amplitude with f^* for free vibrations for the 1 % blockage is shown in figure 8. Figures 3(a) and 6 have been utilized to plot this figure. The data for critical amplitude of oscillation for forced vibrations, shown in figure 7, are also replotted in figure 8. To incorporate the Re effect to some extent, we use the data for $Re = 100$ in figure 7 for plotting the branch corresponding to $Re < 100$ in figure 8. Similarly, the branch corresponding to $Re > 100$ in figure 8 is compared to the data for $Re = 200$ for forced oscillations.

To aid understanding certain landmark data points are marked in figure 8 with upper case letters. The corresponding points are also marked in a copy of figure 3(a) shown in figure 8 in the inset. For example, point A shows the state of the system at $Re = 70$. It corresponds to a very low-amplitude cylinder response and $f^* \sim 1$. Along A-B the amplitude of oscillations increases very gradually while f^* holds a value ~ 1. At $Re \sim 81$ the cylinder response exceeds a certain threshold amplitude and a jump in the value of f^* is observed as indicated by states B and C. For the free vibrations this is the onset of synchronization. As seen from figure 6 the vortex shedding frequency is significantly lower than the natural frequency. The states along C-D form the 'initial branch'. Interestingly, for the forced vibrations all these states lie in the region of 'no-lock-in'. At point D the cylinder marginally exceeds the critical amplitude of forced vibrations needed for lock-in. From D to F_2 through E and F_1, the amplitude

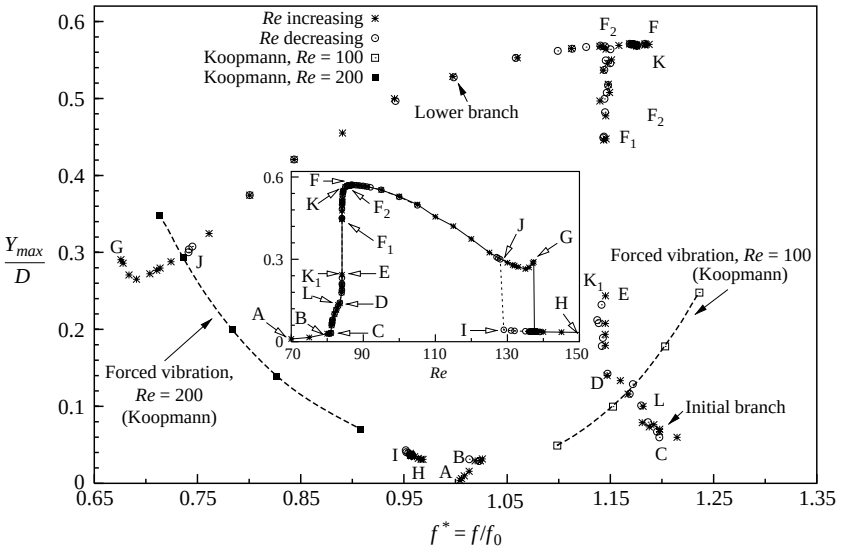

FIGURE 8. Freely vibrating cylinder with 1 % blockage: variation of the amplitude of transverse vibrations with frequency ratio, $f^* = f/f_0$. The data from forced vibrations experiments of Koopmann (1967) from figure 7, and the variation of maximum transverse oscillation amplitude of the cylinder with Re from figure 3 are also shown for comparison.

of vibration increases to the maximum while f^* holds an almost constant value. At F_2 a jump in the vortex shedding frequency (and the vibration frequency) to f_N takes place. During this jump, the amplitude of cylinder response remains almost constant. F is the new state achieved by the system and it marks the onset of the 'lower branch'. All the points along F-G lie on the 'lower branch' and are in a state of 'lock-in'. A slight increase in Re leads to a loss of synchronization and the system achieves the state H. This state is associated with a very low amplitude of cylinder vibrations.

Of interest are the states lying along J-G. These states are associated with a vibration amplitude that is smaller than the threshold value needed for lock-in using the forced vibrations data from Koopmann. Yet synchronization is observed for free vibrations for the Re-increasing computations. Another interesting observation is the manner in which the states along J-G seem to run parallel to the curve for threshold amplitude required for lock-in for forced vibrations.

Let us begin on the decreasing Re branch starting from the point H. Along H-I the cylinder vibration amplitude continues to remain low and is in a no-lock-in state. At I a very slight decrease in Re causes a jump to the lower branch at state J. At this state the vortex shedding frequency is synchronized with the vibration frequency. The amplitude of cylinder oscillations is in excellent agreement with the threshold amplitude required for lock-in for forced vibrations at the corresponding value of f^*. The hysteretic behaviour of the oscillator at the higher Re end of the synchronization is very clear from this figure as well. On further decrease in Re the oscillator exhibits the same behaviour as for increasing Re. It reaches the lower Re end of initial branch through states J-K-F_2-F_1-K_1-D-L-C and remains in the non-synchronized state thereafter.

Essential differences between free and forced vibrations

Figure 8 brings out differences and similarities between free and forced vibrations with respect to synchronization. Excellent agreement is observed between the critical

amplitude of vibrations required for lock-in for free and forced vibrations at the higher Re end of the synchronization. Point J in figure 8 represents the critical amplitude of free vibrations, starting from low-amplitude oscillations, to realize lock-in. This value lies on the curve reported by Koopmann for forced vibrations. However, at the lower Re end of the synchronization the lock-in with free and forced vibrations exhibits a difference. Good agreement is observed between the critical amplitude of cylinder vibrations required for lock-in for forced vibrations and that of free vibrations at which the vortex shedding frequency jumps close to the natural frequency of the oscillator (point D). However, lock-in for free vibrations also exist for lower amplitude along C-D. The vortex shedding frequency in this regime is, of course, significantly different from the natural frequency of the oscillator.

Effect of initial conditions on lock-in

The effect of initial conditions on the lock-in behaviour for free vibrations is also apparent from figure 8. The synchronization regime is extended if the cylinder is already associated with high-amplitude oscillations. This is more prominent for $f^* < 1$ where a part of the curve G-J for free vibrations runs almost parallel to the lock-in boundary for forced vibrations. This suggests that the forced vibrations might be associated with a hysteresis as well. In the original work by Koopmann (1967), the data for forced vibrations were generated by slowly increasing the displacement amplitude of the cylinder while holding the vibration frequency constant. This needs further investigation.

8. Vortex shedding modes

The response of the cylinder follows different branches with variation of Re. These branches are associated with different modes of vortex shedding. Brika & Laneville (1993) reported a mode change from 2S in the initial region to 2P in the lower region of the response of the cylinder. It has been confirmed by the flow visualization studies of Brika & Laneville (1993) and Williamson & Roshko (1988) that hysteresis in the cylinder response is the result of drastic change in the structure of vortices. At low Reynolds number, in the laminar regime, Singh & Mittal (2005) found that the mode of vortex shedding is primarily 2S. However, a variation of this mode, C(2S), is observed when the cylinder undergoes high-amplitude oscillations. The jump in the cylinder response is accompanied by a change in vortex shedding mode: 2S at low and C(2S) at high oscillation amplitudes. They also reported the existence of a P+S mode of vortex shedding (a single vortex and one pair of counter-rotating vortices are released in each cycle of shedding) at $Re \sim 300$ and larger.

8.1. *Overview of the flow*

Instantaneous vorticity fields at various Re are shown in figure 9. At low amplitudes of transverse oscillations, the classical Kármán shedding (2S) is observed. In the 2S mode of shedding, a single vortex is alternately shed from each side of the cylinder during a vortex shedding cycle. Once the cylinder response jumps to the lower branch it begins to oscillate with large amplitude. The vortices in the wake coalesce giving rise to the C(2S) mode of vortex shedding. This can be seen, for example, at $Re = 86$. At this point the vortex shedding frequency approximately matches the natural frequency of the body (see figure 6). In the regime $86 < Re < 137$, the non-dimensional vortex shedding frequency reduces with increase in Re. This can also be observed from the increase in the longitudinal spacing between the vortices in figure 9. $Re \sim 137$ marks the end of synchronization and the longitudinal spacing between the vortices reduces

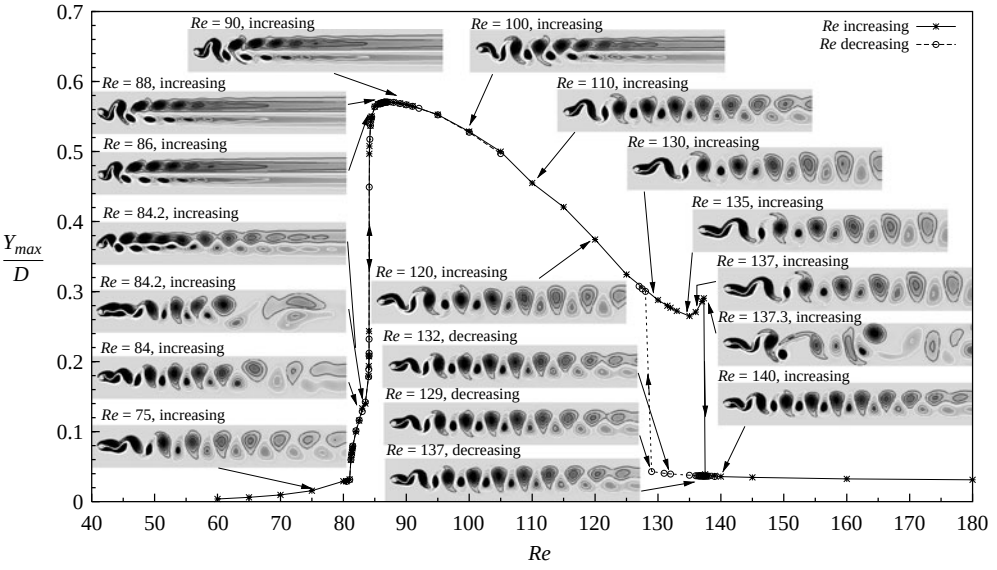

FIGURE 9. Instantaneous vorticity field at various values of Re for the 1 % blockage. For reference, the variation of the transverse amplitude of vibration of the cylinder with Re is also shown.

once again. The flow structure for $Re > 137$ is very similar to that for flow past a stationary cylinder.

Close to the transition between the initial and lower branches of response the flow is associated with both 2S and C(2S) modes of vortex shedding. The 2S mode occurs for the low-amplitude response of the cylinder while the C(2S) mode is seen when the cylinder vibrates with larger amplitude (for example, flow pictures at two different time instants corresponding to low- and high-amplitude vibrations are shown at $Re = 84.2$ in figure 9). It is observed that with high blockage only one of the two modes can occur. Consequently, depending on the initial conditions high- or low-amplitude oscillations may be realized. This leads to hysteresis. For the low blockage a switch between the two modes of vortex shedding takes place. Therefore, the transition is not hysteretic but intermittent.

8.2. *Mode switching*

We investigate, in more detail, the transition from the initial to lower branch for the low blockage. The cases with 1 % and 2.5 % blockage display the same behaviour. Compared to $B = 1$ %, since the computational domain is smaller for the 2.5 % blockage, the computational effort required is a little less. Therefore, we report results for $B = 2.5$ %. Figure 10 shows the time histories of the cylinder response and lift coefficient at certain Re during the transition from the initial to lower branch. The variation of maximum and r.m.s. value of the transverse amplitude of cylinder oscillations and lift coefficient with Re are also shown in the figure. Although the maximum value of the cylinder response and lift coefficient show a jump the variation of the r.m.s. value, with Re, is comparatively gradual.

Figure 10(a) shows the time histories for $Re = 83.2$, which corresponds to almost the end of the initial branch. The cylinder oscillations are of fairly low amplitude. The 2S mode of vortex shedding is observed at all times. Figure 10(b) corresponds to $Re = 83.3$. A sharp increase in the maximum values of the lift coefficient and cylinder

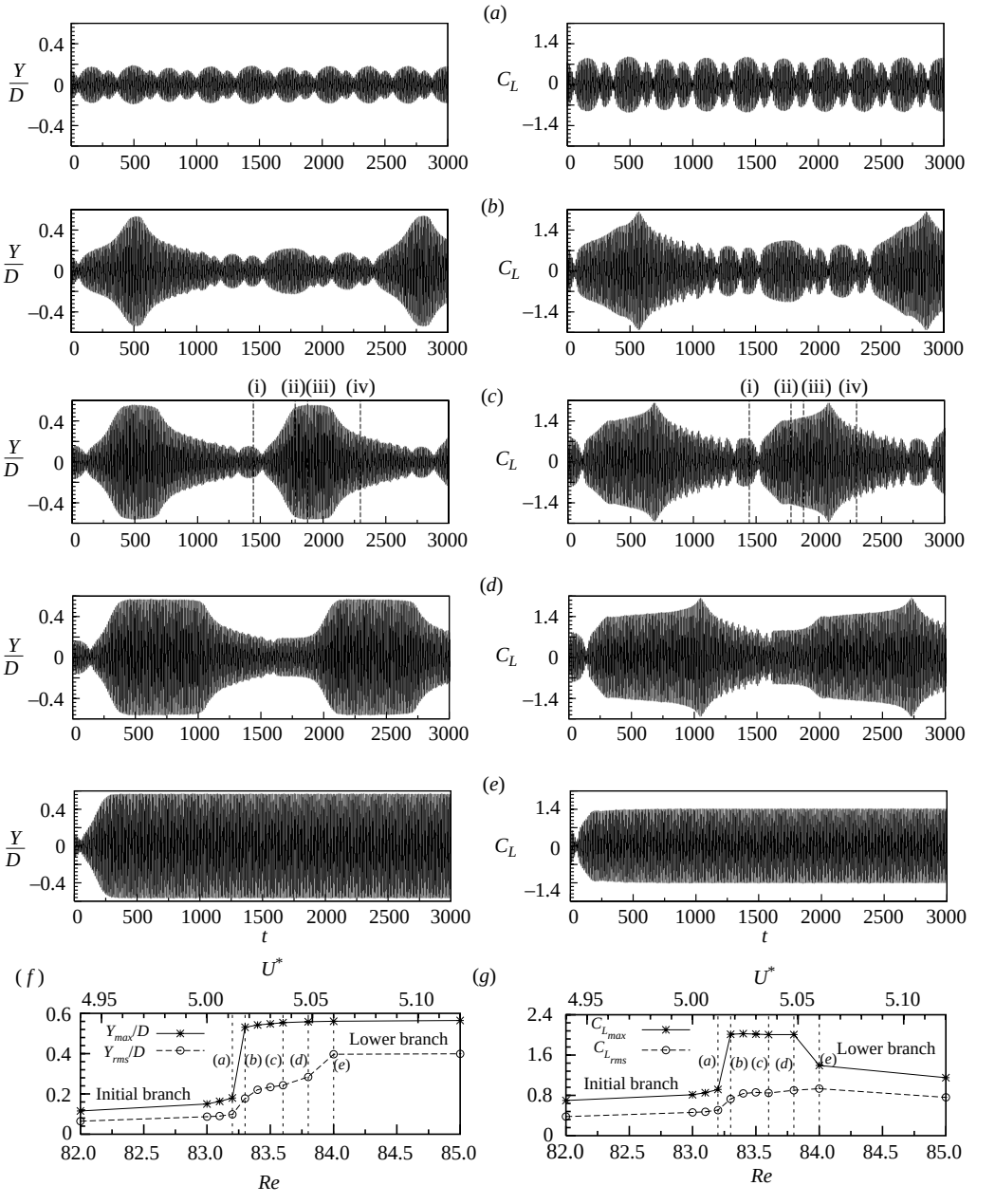

FIGURE 10. Time histories of the transverse response of the cylinder and lift coefficient for the 2.5 % blockage at various Re during the transition from the initial to lower branch. (*a*) $Re = 83.2$, (*b*) $Re = 83.3$, (*c*) $Re = 83.6$, (*d*) $Re = 83.8$, (*e*) $Re = 84$. The variation of the maximum and r.m.s. values of the cylinder response and C_L with Re is also shown in (*f*) and (*g*).

amplitude is observed. The cylinder vibrates with a low amplitude of oscillation most of the time. However, occasionally it undergoes high-amplitude oscillations. As the Reynolds number is increased further, the cylinder undergoes high-amplitude oscillations more frequently. Also, the fraction of time during which the cylinder

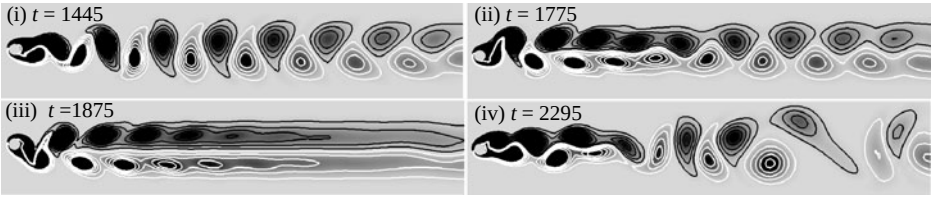

FIGURE 11. $B = 2.5\,\%$, $Re = 83.6$ flow past a freely vibrating cylinder: vorticity field at various time instants. The time instants are marked on figure 10(c).

undergoes high-amplitude oscillations increases. This trend continues up to $Re = 83.8$. At $Re = 84$ the cylinder vibrates with high-amplitude oscillations only. This marks the complete transition to the lower branch.

Figure 11 shows the vorticity field for $Re = 83.6$ at certain time instants that are marked on the time histories of Y/D and C_L in figure 10. The first frame in figure 11 corresponds to a time instant when the cylinder undergoes relatively low-amplitude oscillations. The mode of vortex shedding is 2S. The frame corresponding to point (iii) shows the C(2S) mode of vortex shedding. It is seen from figure 10 that at this time instant the cylinder is undergoing large-amplitude oscillations. At time instants corresponding to points (ii) and (iv) the flow can be seen to be switching between the 2S and C(2S) modes. A similar observation is made at other Re in the transitional regime.

It is seen in figure 11 that the longitudinal spacing between the vortices in the 2S and C(2S) modes of vortex shedding is slightly different. To confirm this, a frequency analysis of the time series for $Re = 83.9$ and 84 is carried out. Figure 12(a) shows the time histories of the cylinder response for the two Reynolds numbers. Shown in figure 12(b) is the variation of the non-dimensional frequency for these time histories based on the time period of each cycle. For $Re = 84$, the frequency does not change and stays close to F_N. However, a variation in frequency is observed for $Re = 83.9$. This is also confirmed from figure 12(c) which shows the time histories of the frequency of C_L obtained by using the Hilbert transform. This is consistent with our earlier observation of the change in the frequency of vortex shedding (and cylinder response) for the low- versus high-amplitude cylinder oscillations in the transitional regime. A similar behaviour was reported by Khalak & Williamson (1999) in their experiments for higher Re for the transition from the upper to lower branch. The power spectra of the time histories of the lift coefficient are shown in figure 12(d). The presence of two frequencies for $Re = 83.9$ is confirmed from this analysis as well. This analysis, therefore, confirms the switching between the two modes of vortex shedding for free vibrations for low blockage.

9. The phase, ϕ, between C_L and Y

We compute the phase, ϕ, between the lift force and transverse cylinder displacement by using the Hilbert Transform on the time histories for the lift force and displacement. Details on the use of this technique can be found in the Khalak & Williamson (1999). Figure 13 shows the variation of phase with Re for 1 % blockage. The variation of the amplitude of cylinder vibrations is plotted alongside. Up to $Re \sim 110$ the lift is almost in phase with the transverse motion of the cylinder. A jump to $\phi \sim 180^\circ$ takes place at $Re \sim 110$. Interestingly, the jump seems to take place exactly in the middle of the synchronization regime. This behaviour is similar to the observation of Khalak &

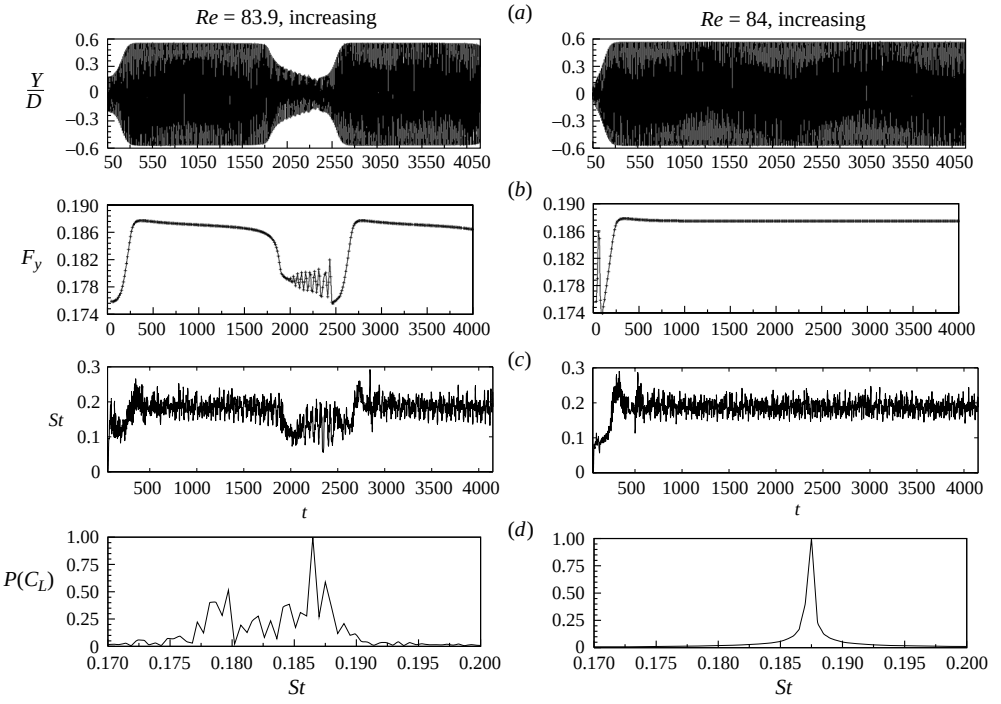

FIGURE 12. $B = 2.5\,\%$, $Re = 83.9$ and 84 flow past a freely vibrating cylinder: time history of (a) the transverse response of the cylinder, (b) its frequency calculated from the time period of each cycle, (c) the frequency of C_L calculated using Hilbert transform, and (d) the power spectra using a fast Fourier transform on the time history of C_L.

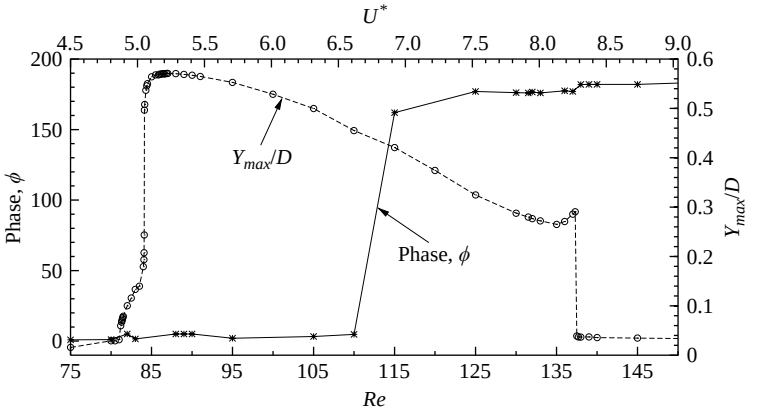

FIGURE 13. The variation of phase, ϕ, between the lift force and transverse displacement of the cylinder with Re for 1 % blockage. For reference the variation of the maximum amplitude of the transverse response of the cylinder is also shown.

Williamson (1999) from their experiments at higher Re. They found that the jump in phase is accompanied by a shift from the upper to lower branch of cylinder response. For low Re there is no upper branch and, therefore, in the present case the cylinder continues to remain on the lower branch. Govardhan & Williamson (2000) have shown that for a freely vibrating cylinder with low mass-damping ($m^*\zeta$), the phase

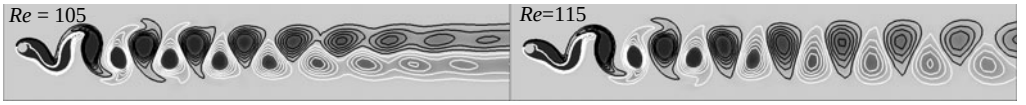

FIGURE 14. $B = 1\,\%$ flow past a freely vibrating cylinder: vorticity plots before ($Re = 105$) and after ($Re = 115$) the phase jump. The cylinder is at the peak of oscillation in both cases.

jump is not associated with a sudden change in the timing of vortex formation. Our computations show that this is true for much smaller Re as well. The phase jump is not hysteretic; the same behaviour is observed for increasing as well as decreasing Re.

It is seen from the close-up view in figure 6(b) that the frequency ratio f/f_N achieves a value of 1.0 at $Re \sim 110$. This is also the Reynolds number at which the jump in phase occurs (see figure 13). The experiments by Govardhan & Williamson (2000) also show that the jump in total phase, ϕ_{total}, takes place when the oscillation frequency is equal to the natural frequency of the structure in vacuum. Note that this behaviour is intrinsic to a linear oscillator of natural frequency f_N which is being forced at frequency f. It can be shown that the expression for the amplitude of the oscillations is inversely proportional to $(1 - f/f_N)$. Therefore, the phase between the force and displacement is expected to show a jump of 180° when the frequency ratio, f/f_N, is increased beyond 1.0.

In forced-vibration studies the jump in phase between the lift force and the transverse cylinder displacement is accompanied by switching of vortex shedding from one side of the cylinder to the other (Ongoren & Rockwell 1988a, b; Carberry *et al.* 2001; Gu *et al.* 1994; Lu & Dalton 1996). It is seen from figure 14 that unlike the forced-oscillation studies, there is no substantial change in the vortex shedding from the cylinder before and after the phase jump in free vibration. If the mode of shedding does not change abruptly, how does the phase jump take place? What are the implications of this jump for free vibrations? We attempt to answer these questions next.

9.1. *How does the phase jump take place?*

On the lower branch of cylinder response, the power spectra of the time histories of the lift coefficient show an additional frequency: $\sim 3St$ (3 times the Strouhal frequency). The component of C_L corresponding to $3St$ becomes stronger as Re approaches 115. In fact, at $Re \sim 115$ the component of C_L corresponding to $3St$ is larger than the one at St, but then decreases compared to the component at St as Re increases further beyond 115. Figure 15 shows the time histories of the lift coefficient for one cycle of the fully developed free vibrations at $Re = 90$, 105, 115 and 125. The presence of a component corresponding to $3St$ leads to two additional local peaks in the time history of the lift force. The contribution from $3St$ overshadows the one from St at $Re = 115$ leading to a change in phase. The cylinder response, also shown in figure 15, in all the cases is almost sinusoidal.

We decompose the total lift force, C_{LT}, in two parts: the viscous, C_{LV} and pressure, C_{LP}, contributions. Figure 15 shows the pressure and viscous components of the total lift force for one cycle of cylinder vibration. The viscous component of lift appears to primarily vary with a frequency corresponding to St and maintains its phase with cylinder motion. However, the pressure component shows a contribution at frequency $3St$ and phase change at $Re \sim 115$.

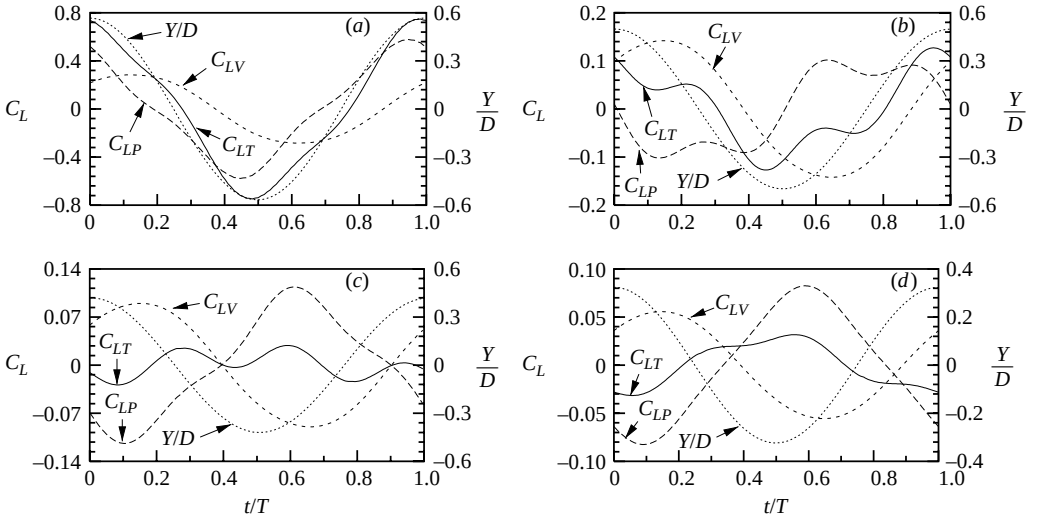

FIGURE 15. $B = 1\,\%$ flow past a freely vibrating cylinder: the time variation of the contributions of the pressure, C_{LP}, and viscous part, C_{LV}, to the total lift coefficient, C_{LT}, during one cycle of the transverse cylinder motion (also shown). (*a*) $Re = 90$, (*b*) $Re = 105$, (*c*) $Re = 115$, (*d*) $Re = 125$.

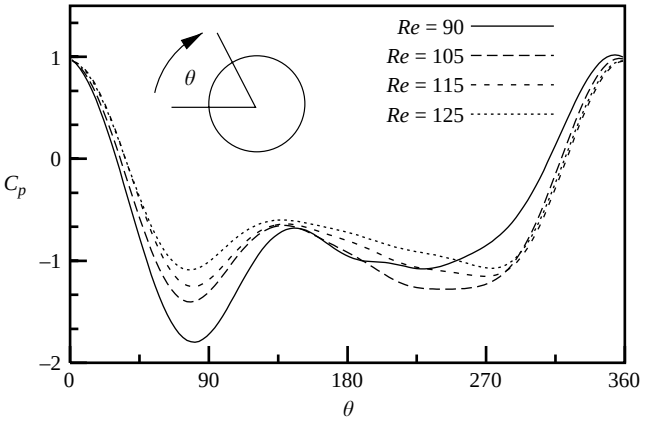

FIGURE 16. $B = 1\,\%$ flow past a freely vibrating cylinder: variation of the pressure coefficient, C_p, on the surface of the cylinder at different Re at a time instant corresponding to the maximum displacement of the cylinder.

Figure 16 shows the variation of pressure coefficient, C_p, on the surface of the cylinder at various Reynolds numbers at a time instant when the cylinder is at its peak displacement. As was also pointed out by Lu & Dalton (1996), C_p attains a value larger than 1 at some points on the surface of the vibrating cylinder. The pressure variation on the cylinder surface can be divided in three regions: the front stagnation point with high C_p and the top and bottom of the cylinder with low C_p (Stewart *et al.* 2005). The appearance of phase shift in C_{LP} is primarily caused by the movement of these three pressure regions and their relative values. From figure 16 it can be seen that the location of the stagnation point and the maximum suction on the upper surface of the cylinder is virtually the same for all the Re shown. The maximum

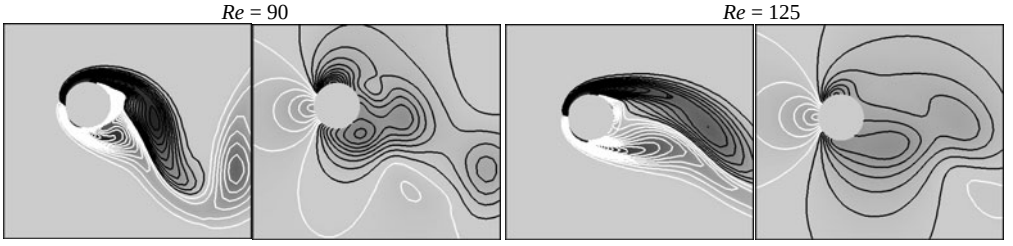

FIGURE 17. $B = 1\,\%$ flow past a freely vibrating cylinder: instantaneous vorticity (left) and pressure (right) fields before ($Re = 90$) and after ($Re = 125$) the phase jump. The cylinder is at peak amplitude of oscillation in both cases.

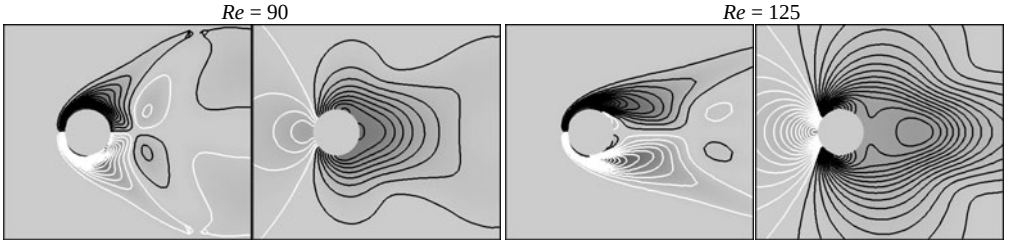

FIGURE 18. $B = 1\,\%$ flow past a freely vibrating cylinder: vorticity (left) and pressure (right) fields for the time-averaged flow for $Re = 90$ and 125.

suction on the upper surface occurs close to the shoulder of the cylinder. However, the location of maximum suction on the lower surface of the cylinder is quite different for the four Re. Compared to $Re = 105$, the maximum suction at $Re = 125$ is smaller and occurs closer to the shoulder of the cylinder. This leads to an overall negative value of C_{LP} for $Re = 125$ and a positive value for $Re = 105$. Thus, the total lift at $Re = 125$ becomes out of phase with the cylinder motion.

In order to further investigate the phenomenon of phase jump we decompose the flow into two components: the time average, $(\bar{\boldsymbol{u}}, \bar{p})$, and perturbation, $(\boldsymbol{u}', p')$. At any time instant, $(\boldsymbol{u}, p) = (\bar{\boldsymbol{u}}, \bar{p}) + (\boldsymbol{u}', p')$. We choose two Re for the study, 90 and 125, which lie on either side of the phase jump. Figure 17 shows the instantaneous vorticity and pressure fields at a time instant when the cylinder is at its peak amplitude of oscillation. Compared to $Re = 125$, at $Re = 90$ the oscillation amplitude of cylinder as well as St is much larger (figures 3 and 6). Therefore, the transverse speed of the cylinder is significantly larger for $Re = 90$. As a result, the vibrating cylinder experiences a more intense movement of the stagnation point as well as the suction peaks for $Re = 90$ than $Re = 125$. Also, at $Re = 90$, the vortices are stronger and the cylinder is associated with a wake of larger lateral width. Figure 18 shows the time-averaged flow for the two Re. The variation of $\bar{C}_p$ along the cylinder surface is also shown in figure 19(a). Unlike the wake of a stationary cylinder, a set of counter-rotating vortices is observed in the near wake of the time-averaged flow of the vibrating cylinder. A similar observation on the average vorticity was made by Govardhan & Williamson (2001) for the 2P mode at much higher Re ($Re = 3900$). The proximity of the counter-rotating vortices to the base of the cylinder at $Re = 90$ leads to an additional peak in $\bar{C}_p$.

The intense movement of the stagnation and peak suction points for the $Re = 90$ case results in a value of $\bar{C}_p$ much lower than unity at $\theta = 0$. Additionally, the base

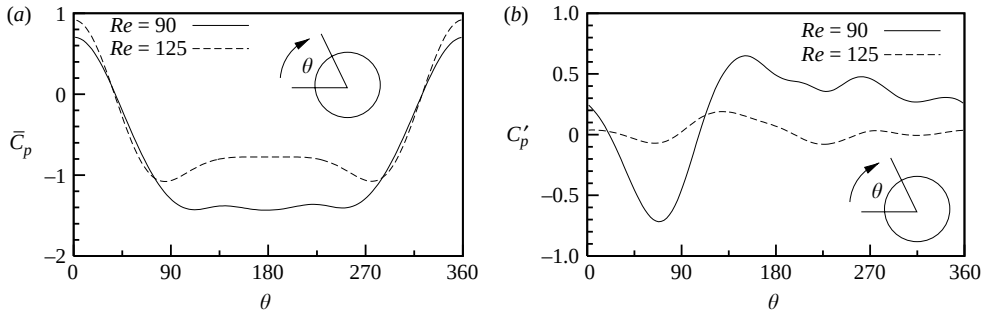

FIGURE 19. $B = 1\,\%$ flow past a freely vibrating cylinder: variation of (a) mean pressure coefficient, $\bar{C}_p$ and (b) perturbation pressure coefficient, C'_p, on the surface of the cylinder when it is at its peak amplitude of oscillation for $Re = 90$ and 125.

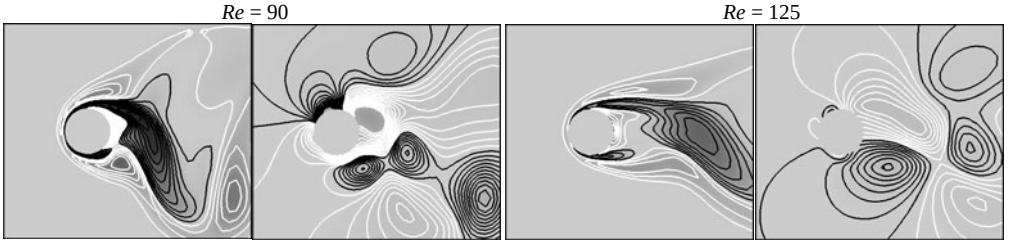

FIGURE 20. $B = 1\,\%$ flow past a freely vibrating cylinder: The perturbation vorticity (left) and pressure fields (right) for $Re = 90$ and 125. The cylinder is at peak amplitude of oscillation in both cases.

suction at $Re = 90$ is much larger than that at $Re = 125$ as is clearly visible from figure 19(a). In general, the mean pressure is much lower for the $Re = 90$ flow. Of the two, the $\bar{C}_p$ distribution for the vibrating cylinder at $Re = 125$ is much closer to the one observed for a stationary cylinder. Figure 20 shows the perturbation fields for vorticity and pressure when the cylinder is at peak amplitude of oscillation for the two Re. The footprint of the time-averaged flow can clearly be seen in these pictures. Significant differences can be observed between the two set of results. The perturbation field for $Re = 125$ is similar to that observed for a stationary cylinder. However, the $Re = 90$ field clearly shows more flow structures. This is perhaps the cause of the occurrence of the $3St$ harmonic in the time variation of lift forces. The variation of C'_p along the cylinder surface is shown in figure 19(b). This clearly brings out the difference between the two cases. While the pressure coefficient shows suction at the lower surface for $Re = 125$, it remains positive on the entire lower surface of the cylinder at $Re = 90$. In addition, the suction on the upper surface is significantly larger for $Re = 90$. Consequently, at its peak transverse location, a positive lift is experienced by the cylinder for $Re = 90$ while is is negative for $Re = 125$. This shows that the cylinder motion and lift are in phase for $Re = 90$ and out of phase at $Re = 125$.

9.2. *Implications of the phase jump for free vibrations*

Our computations of free vibrations give us the time histories of the cylinder response and forces. The phase between the lift and transverse displacement can be found from the time histories. It is possible to utilize the time history of the lift coefficient obtained from the computations to solve for the cylinder response by integrating (2.7). By doing

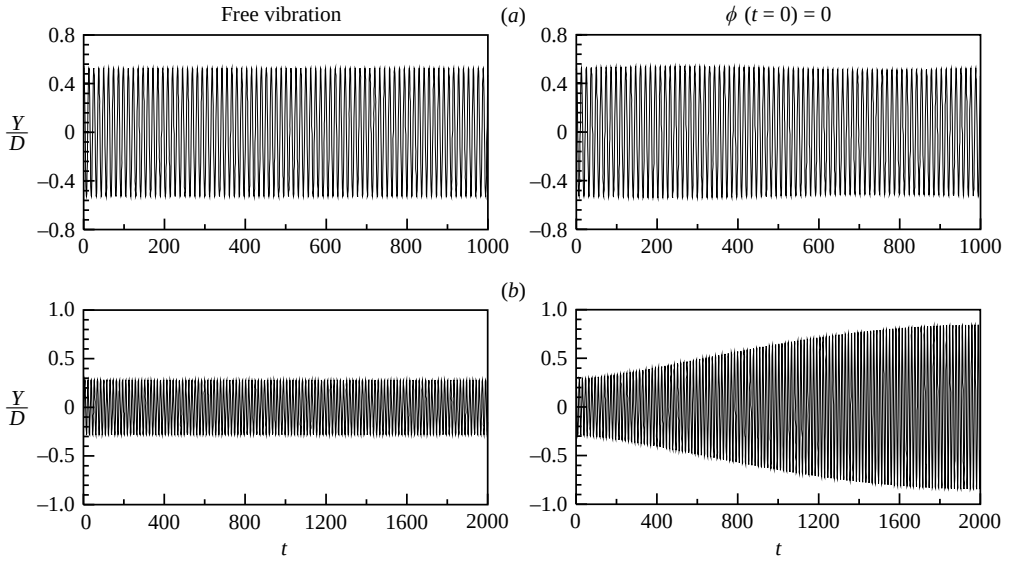

FIGURE 21. $B = 1\,\%$, (*a*) $Re = 100$ and (*b*) 130 flow past a freely vibrating cylinder: effect of the phase difference between the lift force and cylinder displacement on the cylinder response. The left column shows the results from free vibrations. The right column shows the results for a computation where the phase is forced to be zero at $t = 0$ while the data for the aerodynamic coefficients from the free vibration study are utilized.

this we recover the time history of the cylinder response from the free vibrations. To investigate the effect of the phase shift between the lift and cylinder displacement we manipulate the initial condition (cylinder displacement and speed) so that at $t = 0$ the lift and cylinder displacement are in phase. Equation (2.7) is then integrated by starting from the changed initial condition and using the time history for the C_L from free vibrations. The time histories of the cylinder response for free vibrations and with $\phi(t = 0) = 0$ are shown in figure 21. Figure 21(*a*) shows results for $Re = 100$ while figure 21(*b*) is for $Re = 130$. At $Re = 100$, where the lift and cylinder response are almost in phase during free vibrations, the effect of forcing the initial phase to zero is not significant. However, at $Re = 130$ where the lift and cylinder response are out of phase in free vibrations, forcing $\phi(t = 0) = 0$ leads to very large-amplitude oscillations of the cylinder. This suggests that the phase shift between the lift force and cylinder displacement is essentially a mechanism to limit the oscillation amplitude of the cylinder.

Several researchers have looked at the energy transfer between the oscillator and fluid. In forced vibration studies, the phase shift between the lift force and the transverse cylinder displacement is associated with a change in the direction of energy transfer (Carberry *et al.* 2001; Blackburn & Henderson 1999; Stewart *et al.* 2005). The present computations have been carried out with zero structural damping. Since the flow and the response are periodic, therefore, there is no net energy transfer per cycle between the fluid and the oscillator.

10. Conclusions

Results have been presented for the free vibrations of a circular cylinder of low non-dimensional mass ($m^* = 10$) in the regime of laminar flow ($60 < Re < 200$). The

computations have been carried out in two dimensions using a stabilized finite element method. Lock-in/synchronization is observed for a wide range of Reynolds numbers. Two branches of cylinder response are identified: initial and lower. These branches have been established by other investigators for higher Re flow in earlier research. While the initial branch is associated with low-amplitude vibrations, the cylinder vibrates with relatively large amplitude on the lower branch. The maximum amplitude of transverse vibrations of the cylinder is $\sim 0.6D$. The vortex shedding pattern on the initial branch is 2S. It is C(2S) on the lower branch. Hysteresis behaviour near the lower-Re end of lock-in depends on the blockage. As the blockage is reduced the size of the hysteresis loop decreases. For blockage of 2.5 % and less the hysteretic behaviour disappears. Instead, the transition from the initial to the lower branch is intermittent. A switching between the $2S$ and $C(2S)$ modes of vortex shedding is observed in this transitional regime. The mode of shedding is $2S$ when the cylinder exhibits low-amplitude oscillations. It switches to the $C(2S)$ mode when the amplitude of oscillations is large. Also, the frequency of cylinder oscillations and vortex shedding is marginally larger when the mode of shedding is $C(2S)$. This is confirmed via a frequency analysis of the time histories of the cylinder response by using Fourier and Hilbert transforms.

A comparison of free vibration results with experimental data for forced vibrations from an earlier study is carried out. Excellent agreement for the critical amplitude required for onset of synchronization is observed. The comparison brings out certain interesting observations. There is a possibility that the lock-in behaviour in forced vibration is sensitive to the initial condition, i.e. a hysteresis might exist. This needs further investigation. Another observation is that the initial branch for free vibrations seems to lie outside the lock-in region predicted by forced vibrations. It should be noted though that in the free vibrations the cylinder vibration frequency is lower than the natural frequency on the initial branch.

The phase angle between lift force and transverse displacement of the cylinder shows a jump of approximately 180° at the middle of the synchronization region. The jump in phase is found to occur at a point where the frequency ratio f/f_N attains the value 1.0. The jump in phase is not hysteretic in nature. It is also not associated with any radical change in shedding pattern. Decomposing the total lift force into viscous and pressure components at various Re reveals that the jump in phase is caused by the pressure component. The viscous component, on the other hand, maintains its phase with cylinder motion at all Re. Three important regions with respect to the pressure are identified. They are the front stagnation point, and the suction on the upper and lower sides of the cylinder. The change in the phase of the pressure component is caused by the movement of these three pressure regions over the surface of the cylinder and a variation in their relative magnitude. To further understand the phenomenon of phase jump, decomposition of the flow into time-averaged and perturbation components has been carried out. The time-averaged flow before ($Re = 90$) and after ($Re = 125$) the phase jump shows interesting differences. While the $Re = 125$ flow is similar to the mean flow past a stationary cylinder, the $Re = 90$ flow shows a pair of counter-rotating vortices in the near wake. In general, the $\bar{C}_p$ distribution shows a lower value along the cylinder surface for the $Re = 90$ flow. The perturbation field for the $Re = 90$ flow shows more vortex structures, compared to that at $Re = 125$, close to the cylinder. The C_p' distribution clearly brings out the flow features responsible for the phase jump. The jump in the phase appears to be a mechanism to self-limit the maximum amplitude of oscillation of the cylinder.

Partial support for this work from the Department of Science and Technology, India is gratefully acknowledged.

REFERENCES

Al Jamal, H. & Dalton, C. 2005 The contrast in phase angles between forced and self-excited oscillations of a circular cylinder. *J. Fluids Struct.* **20**, 467–482.

Bearman, P. W. 1984 Vortex shedding from oscillating bluff bodies. *Annu. Rev. Fluid Mech.* **16**, 195–222.

Bishop, R. E. D. & Hassan, A. Y. 1964 The lift and drag forces on a circular cylinder oscillating in a flowing fluid. *Proc. R. Soc. Lond.* A **277**, 51–75.

Blackburn, H. M & Henderson, R. D. 1999 A study of two-dimensional flow past an oscillating cylinder. *J. Fluid Mech.* **385**, 255–286.

Brika, D. & Laneville, A. 1993 Vortex induced vibrations of long flexible circular cylinder. *J. Fluid Mech.* **250**, 481–508.

Carberry, J., Sheridan, J. & Rockwell, D. 2001 Forces and wake modes of an oscillating cylinder. *J. Fluids Struct.* **15**, 523–532.

Carberry, J., Sheridan, J. & Rockwell, D. 2005 Controlled oscillations of a cylinder: forces and wake modes. *J. Fluid Mech.* **538**, 31–69.

Feng, C. C. 1968 The measurement of vortex-induced effects in flow past a stationary and oscillating circular cylinder and d-section cylinders. Master's Thesis, University of British Columbia.

Govardhan, R. & Williamson, C. H. K. 2001 Mean and fluctuating velocity fields in the wake of a freely-vibrating cylinder. *J. Fluids Struct.* **15**, 489–501.

Govardhan, R. & Williamson, C. H. K. 2000 Modes of vortex formation and frequency response of a freely vibrating cylinder. *J. Fluid Mech.* **420**, 85–129.

Gu, W., Chyu, C. & Rockwell, D. 1994 Timing of vortex formation from an oscillating cylinder. *Phys. Fluids* **6**, 3677–3682.

Henderson, R. D. 1995 Details of the drag curve near the onset of vortex shedding. *Phys. Fluids* **7**, 2102–2104.

Khalak, A. & Williamson, C. H. K. 1996 Dynamics of a hydroelastic cylinder with very low mass and damping. *J. Fluids Struct.* **10**, 455–472.

Khalak, A. & Williamson, C. H. K. 1999 Motion, forces and mode transitions in vortex-induced vibrations at low mass damping. *J. Fluids Struct.* **13**, 813–851.

Koopmann, G. H. 1967 The vortex wakes of vibrating cylinders at low Reynolds numbers. *J. Fluid Mech.* **28**, 501–512.

Kumar, B. & Mittal, S. 2006*a* Effect of blockage on critical parameters for flow past a circular cylinder. *Intl J. Numer. Meth. Fluids.* **50**, 987–1001.

Kumar, B. & Mittal, S. 2006*b* Prediction of the critical Reynolds number for flow past a circular cylinder. *Comput. Meth. Appl. Mech. Engng* **195**, 6046–6058.

Leontini, J. S., Thompson, M. C & Hourigan, K. 2006 The beginning of branching behaviour of vortex-induced vibration during two-dimensional flow. *J. Fluids Struct.* **22**, 857–864.

Lu, X. Y., Dalton, C. 1996 Calculation of the timing of vortex formation from an oscillating cylinder. *J. Fluids Struct.* **10**, 527–541.

Mittal, S. 1992 Stabilized space-time finite element formulation for unsteady incompressible flows involving fluid-body interaction. PhD thesis, University of Minnesota.

Mittal, S. & Kumar, V. 1999 Finite element study of vortex- induced cross-flow and in-line oscillations of a circular cylinder at low Reynolds numbers. *Intl J. Numer. Meth. Fluids.* **31**, 1087–1120.

Mittal, S. & Kumar, V. 2001 Flow induced oscillations of two cylinders in tandem and staggered arrangement. *J. Fluids Struct.* **15**, 717–736.

Mittal, S. & Singh, S. 2005 Vortex-induced vibrations at subcritical *Re*. *J. Fluid Mech.* **534**, 185–194.

Mittal, S. & Tezduyar, T. E. 1992 A finite element study of incompressible flows past a oscillating cylinders and airfoils. *Intl J. Numer. Meth. Fluids* **15**, 1073–1118.

Norberg, C. 2003 Fluctuating lift on a circular cylinder: review and new measurement. *J. Fluids Struct.* **17**, 57–96.

Ongoren, A. & Rockwell, D. 1988*a* Flow structure from an oscillating cylinder Part 1. Mechanisms of phase shift and recovery in the near wake. *J. Fluid Mech.* **191**, 197–223.

Ongoren, A. & Rockwell, D. 1988*b* Flow structure from an oscillating cylinder Part 2. Mode competition in the near wake. *J. Fluid Mech.* **191**, 225–245.

Parkinson. G. V. 1989 Phenomena and modelling of flow-induced vibrations of bluff bodies. *Prog. Aerospace Sci.* **26**, 169–224.

Prasanth, T. K., Behara, S., Singh, S. P., Kumar, R. & Mittal, S. 2006 Effect of blockage on vortex-induced vibrations at low Reynolds numbers. *J. Fluids Struct.* **22**, 865–876.

Sarpkaya, T. 1979 Vortex-induced oscillations – a selective review. *J. Appl. Mech.* **46**, 241–258.

Sarpkaya, T. 2004 A critical review of the intrinsic nature of vortex-induced vibrations. *J. Fluids Struct.* **19**, 389–447.

Singh, S. P. & Mittal, S. 2005 Vortex-induced oscillations at low Reynolds numbers: hysteresis and vortex shedding modes. *J. Fluids Struct.* **20**, 1085–1104.

Stansby, P. K. 1976 The locking-on of vortex shedding due to the cross-stream vibration of circular cylinders in uniform and shear flows. *J. Fluid Mech.* **74**, 641–665.

Stewart, B. E., Leontini, J. S., Hourigan, K. & Thompson, M. C. 2005 A numerical survey of wake modes and energy transfers for an oscillating cylinder at Re=200. *Fourth Symposium on Bluff Body Wakes and Vortex-Induced Vibrations, Greece* (ed. T. Leweke & C. H. K. Williamson), pp. 239–242.

Tezduyar, T. E., Behr, M. & Liou, J. 1992*a* A new strategy for finite element computations involving moving boundaries and interfaces- the deforming-spatial-domain/space–time procedure, I: the concept and the preliminary tests. *Comput. Meth. Appl. Mech. Engng* **94**, 339–351.

Tezduyar, T. E., Behr, M., Mittal, S. & Liou, J. 1992*b* A new strategy for finite element computations involving moving boundaries and interfaces- the deforming-spatial-domain/space–time procedure, II: computations of free-surface flows, two liquid flows and flows with drifting cylinders. *Comput. Meth. Appl. Mech. Engng* **94**, 353–371.

Tezduyar, T. E., Mittal, S., Ray, S. E. & Shih, R. 1992*c* Incompressible flow computations with stabilized bilinear and linear equal-order-interpolation velocity pressure elements. *Comput. Meth. Appl. Mech. Engng* **95**, 221–242.

Williamson, C. H. K. & Govardhan, R. 2004 Vortex induced vibration. *Annu. Rev. Fluid Mech.* **36**, 413–455.

Williamson, C. H. K. & Roshko, A. 1988 Vortex formation in the wake of an oscillating cylinder. *J. Fluids Struct.* **2**, 355–381.